

# A Large-Scale Epidemic Simulation Framework for Realistic Social Contact Networks

Joy Kitson\*, Ian Costello\*, Jiangzhuo Chen<sup>†</sup>, Diego Jiménez<sup>‡</sup>, Stefan Hoops<sup>†</sup>, Henning Mortveit<sup>†</sup>, Esteban Meneses<sup>‡</sup>, Jae-Seung Yeom<sup>§</sup>, Madhav V. Marathe<sup>†</sup>, Abhinav Bhatele\*

\*University of Maryland, College Park

<sup>†</sup>University of Virginia

<sup>‡</sup>National High Technology Center

<sup>§</sup>Lawrence Livermore National Laboratory

**Abstract**—Global pandemics can wreak havoc and lead to significant social, economic, and personal losses. Preventing the spread of infectious diseases requires implementing interventions at different levels of government, and evaluating the potential impact and efficacy of those preemptive measures. Agent-based modeling can be used for detailed studies of epidemic diffusion and possible interventions. We present Loimos, a highly parallel simulation of epidemic diffusion written on top of Charm++, an asynchronous task-based parallel runtime. Loimos uses a hybrid of time-stepping and discrete-event simulation to model disease spread. We demonstrate that our implementation of Loimos is able to scale to large core counts on an HPC system. In particular, Loimos is able to simulate a US-scale synthetic interaction network in an average of 1.497 seconds per simulation day when executed on 16 nodes on Rivanna, processing around 428 billion interactions (person-person edges) in under five minutes for an average of 1.4 billion traversed edges per second (TEPS).

## I. INTRODUCTION

The COVID-19 pandemic has demonstrated that while we have made significant progress in controlling infectious disease outbreaks, such outbreaks will continue to pose a threat. Computational models played an important role during the COVID-19 pandemic response efforts. The models were used to forecast the trajectory of the pandemic, evaluate various what-if scenarios, and support economic and logistic planning problems such as vaccine allocation and distribution. The CDC forecast hub [17], CDC scenario modeling hub [32], and the efforts by various state health agencies [1], [3] provide excellent examples of how models were used effectively to aid public health decision making in near real-time. Several challenges have also emerged as a result of these efforts; these include: (1) running these models in real time, (2) scaling the model to larger regions and incorporating multiple social, behavioral, economic and immunological considerations and (3) handling the uncertainty produced by limited data regarding conditions on the ground.

Traditional modeling techniques for the spread of infectious diseases rely on coupled rate equations – systems of differential equations relating the number of people who are susceptible, exposed, infected, and recovered (SEIR) [26]. These equations have proved effective at capturing *statistical* trends like the rate at which people are infected. However, such models fail to capture the complexity of human social

networks and the interactions that serve as a mechanism for disease spread. As many interventions function by changing this network of interactions, their impact on a disease’s spread can only be modeled indirectly under this paradigm.

In contrast, agent-based models take a different approach – they simulate the epidemic process on social contact networks that capture the dynamics of human interactions. While more flexible, this approach is much more computationally expensive, requiring agent-based models to be high scalable. The first reason for this, is that it is important to be able to simulate epidemic dynamics over national and global scale networks. A realistic social contact network for the U.S. would have ~290 million agents, and a global scale network would have ~8 billion. Second, interventions are an important component of any epidemic simulation that seeks to study the impact of government planning and response. However, interventions complicate interaction networks that are already highly irregular by allowing them to change over time, which can slow simulations down considerably.

Design and implementation of parallel simulations for contagion modeling is challenging for two main reasons: (1) The underlying social contact networks on which infectious diseases spread are highly unstructured, see [10], [12] for an in depth discussion and (2) the dynamics over such networks are stochastic in nature – this implies that different nodes might participate in the spreading process. Taken together, this makes the task of partitioning and load balancing challenging as one cannot predict the inter-process communication and workload on each processor *a priori*. A few papers have claimed scaling to a large number of nodes but the underlying networks have been highly structured; in some cases, aggregation techniques were used implicitly to reduce the size of the network [8], [36].

Also, a typical epidemiological workflow requires running thousands of simulation replicates. One reason is that many replicates are required to get a tight error bound due to the stochasticity of the underlying simulations. The other reason is to develop ensemble (particle-based) methods to capture the inherent uncertainty in parameter values. A typical design with 20 cells, 30 replicates, and 100 particles can yield 60,000 simulation experiments. Doing this many experiments in a

TABLE I: Summary of prior agent-based epidemic simulator results.

Simulator	People	Simulated Days	Machine	Cores	Runtime	Runtime Per Day
FRED [25]	289 million	Unknown	Blacklight at PSC	16	4 h	Unknown
EpiCast [22]	281 million	180	2.4 GHz Intel Xeon	256	8-12 h	160 s
EpiHiper [11]	288 million	72,000	Bridges-2 at PSC	6,400	32 h 42 m	0.141 s
EpiSimdemics [9]	280.4 million	180	Rivanna at UVA	1,200		
			Blue Waters at NCSA	655,360	10.41 s	0.0578 s

short amount of time requires a highly scalable code. Running such large workflows means pushing the limits of performance, and motivates the development of a parallel program capable of scaling to meet these demands.

Our primary objective in this work is to develop a scalable, parallel simulation framework for modeling contagion processes over large relational and time-varying networked systems. Towards this end, we present Loimos, a highly scalable application for agent-based simulations on realistic social contact networks, written on top of an asynchronous task-based parallel runtime.

### A. Contributions and Significance.

Our key contributions include:

- The design and implementation of a scalable and modular parallel agent-based simulator for modeling contagion processes and intervention scenarios at an individual level. The code is open source and available at <https://github.com/loimos/loimos>.
- A flexible and user-friendly input format based on Google’s Protocol Buffers (Protobuf) library [24] to represent disease models, population datasets, and intervention scenarios.
- Demonstration of the scalability of the code on an HPC platform both in strong and weak scaling scenarios.
- Validation of the simulator against EpiHiper [31], an existing model used by the CDC COVID-19 scenario modeling hub [41].

## II. RELATED WORK

Bissett et al. identify five components to agent-based techniques for modeling epidemics: (1) a theory component, (2) synthetic population construction, (3) social contact network generation from such synthetic populations, (4) construction of idealized social contact networks, and (5) simulation of epidemic diffusion across the both types of contact networks [13]. It is this last component which we focus on in this work and mostly rely upon existing work in the four preceding areas.

There have been several recent publications on modeling the spread of COVID-19. Many of these have been national or regional compartmental models built using data from outbreaks in the simulated area, and account for interventions in different ways. The SIQR (Susceptible Infectious Quarantined Recovered) [40] and SIDARTHE (Susceptible Infected Diagnosed Ailing Recognized Threatened Healed and Extinct) [23] models have been used to simulate the progression of the pandemic in India and Italy, respectively, using new disease

states and adjustments to the values of disease parameters to capture the impact of interventions. An age-segmented SIRD (Susceptible Infectious Recovered Dead) model using synthetic contact matrices for interventions [38] has been used for COVID-19 modelling, as has another SIRD model which used an optimization algorithm to estimate the infection rate based on empirical data [5]. COVID-19 has also been modeled at an international scale using meta-population models, which segment the simulated population into subpopulations representing countries or regions and build a compartmental model for each subpopulation with flows connecting them. One such model was used to estimate the impact of travel restrictions on the early spread of COVID-19 [16]. There have also been some efforts to build small-scale agent-based models to simulate the spread of the virus within small communities or within single buildings. Although these models range in complexity – COVID-ABS incorporates both economic and epidemiological models within a single simulation [39] whereas Cuevas’s model of spread within a building only requires two rules to guide its agents’ behavior [18] – most of these models are quite small, only simulating a few hundred agents.

Several parallel agent-based epidemic simulators have also been developed for HPC systems, including several that operate on national scales. However, any performance comparison between existing models is hampered by the lack of detailed information on the parameters and HPC systems used in the runs. No single ground truth dataset exists to test raw computation speed in this domain, so we instead seek to compare simulations which operate on a similar scale, namely that of the population of the United States.

With this limitation in mind, there are a number of approaches to developing high-performance agent-based disease simulations. The Framework for Replication of Epidemiological Dynamics (FRED) is an OpenMP based simulation that uses US census data to model epidemic simulations [25]. FRED’s disease models are fixed to a configurable SEIR model (susceptible, exposed, infectious, and recovered), resulting in much less flexibility in terms of input, compared to codes which support a tunable arbitrary disease model, such as Loimos. Seal et al. [4] implement an agent-based model involving a generalization of Conway’s Game of Life, which is distinct in both features and purpose from Loimos. However, this simulation is notable for their use of GPU offloading, which most of the simulations surveyed – along with Loimos – do not support. Germann et al. [22] adapt the SPaSM molecular dynamics simulation by using cells as an analog for communities and particles as an analog for individual

agents. The result, EpiCast, sits halfway between a meta-population model with its spacial distributed interaction groups and a fully-fledged agent-based model by placing each agent in multiple interaction groups at once, representing where they live, work, and travel. Parker et al. [35] introduce a novel approach that models how human behavior actually changes due to a pandemic (e.g. increased social distancing) but is limited to an SEIR model and requires interventions to have different populations to model different behaviors. Machin et al. [31] and the EpiHiper team present an agent-based simulator embedded in an end-to-end pipeline which runs the gauntlet from model calibration to analyzing the simulation output [10], which has been used by the CDC COVID-19 scenario modeling hub [41]. While this represents a mature production simulation, their work focuses more on the orchestration of the overall pipeline than the optimization of individual application runs. Eubank et al. [19], Longini et al. [30], and Ferguson et al. [20] present other earlier epidemic simulations.

Some of the fastest epidemic simulations have been performed by Perumalla et al. [37], and by the EpiSimdemics team, with results published at SC 2008 [7], IPDPS 2014 [43], and CCGrid 2017 [9]. EpiSimdemics has shown impressive scaling as per their SCALE submission to CCGrid in 2017 [9], in which they present a zip-code based partitioning scheme similar to the one employed by Loimos. They show orders of magnitude difference in performance compared to previous work and their own work. Table I summarizes the performance of some of the more performant models discussed in this section, and highlights EpiSimdemics' performance lead.

### III. ALGORITHM FOR CONTAGION DIFFUSION

In our epidemic simulator, Loimos, we employed a combination of network theory, discrete event simulations, and agent-based modeling. In this approach, both individuals in the population (referred to as "agents") and interactions between pairs of them are modeled. This framework models the dynamics of epidemic diffusion on a sufficiently granular level for us to model how the dynamics of disease spread change in the presence of a range of public health intervention strategies – like vaccinations and quarantines – which act directly on those dynamics.

#### A. Serial Algorithm

Simulating the evolution of the system requires iterating over discrete time steps. During each time step, we need to

- 1) Identify which people had overlapping visits to the same location.
- 2) Calculate the likelihood that each overlap resulted in an infection, then determine which infections occur, if any.
- 3) Update each person's health state to reflect any infections and the progression of the disease.

1) *Disease Model and Finite State Automaton:* Each person's health state is managed using a finite state automaton (FSA) that specifies how – once infected – people move through various health states. These states represent various

---

#### Algorithm 1: Computing interactions at a location

---

```

1 ComputeInteractions on event queue Q:
2 foreach e ∈ Q do
3   if e is arrival then
4     Put p into visitor list Pv;
5   else
6     Remove p from Pv;
7     foreach p' currently in Pv do
8       /* Contact occurs with fixed
9        probability at a given location */
10      if p and p' have made contact then
11        Compute propensity of infection for p and p'
12        during the period of co-occupancy T;
13        Add interaction to interaction list Ip for p;
14        Add interaction to interaction list Ip' for p';
15      end
16    end
17  end
18 end

```

---

states in the progression of a disease, with each having an associated susceptibility,  $\sigma$ , and infectivity,  $\iota$ , which determine how they are treated in the simulation. Transitions between states are non-deterministic both in terms of the state transitioned to and how long a person remains in a given state. The model used for simulations in this paper is an expanded version of the Susceptible, Exposed, Infectious, and Recovered (SEIR) model (see [29]), tuned to represent COVID-19.

2) *Discrete-event Simulation:* The discrete event simulation (DES) determines which people were at a location  $\ell$  at the same time and for how long. Its input is the list of visits to  $\ell$  during a given simulation day. The DES splits each visit into two events – an arrival and a departure – and orders them in a queue based on the time when they occur. The DES then processes events from this queue as shown in Algorithm 1, identifying all of the interactions between people at  $\ell$  within this timestep.

While processing events, we maintain a list of all people currently at the location, adding a person when they arrive (line 4) and removing them when they depart (line 6). When a person leaves, we consider everyone remaining in the list as potential contacts with a fixed probability based on the location, as outlined in Section III-A3 (lines 8-9). If a contact occurs between an infectious person and a susceptible person, we calculate the propensity of the resulting interaction to cause an infection (line 10) - as per Equation 2. A record of this interaction is then stored for the susceptible person.

3) *Contact Model:* The contact model operates at each location  $\ell$  independently, and determines whether or not any given pair of people with overlapping visits to  $\ell$  come into contact. The general idea is that not every pair of people present at the same location at the same time should actually come into contact at larger locations, but they should at smaller locations.

We formalize this framework as the *min/max/α* model. In this model, we compute the *contact probability*,  $p$ , for any pair of people simultaneously present at that location as a function of its maximum occupancy,  $N$ . This serves as a proxy for its size. In order to compute that value, we select a minimum

occupancy,  $A$ , at or below which everyone will make contact, and a maximum occupancy,  $\alpha$ , at or above which someone visiting at the peak occupancy of the location will make about  $B$  contacts. This means that a person visiting a location during peak occupancy should expect to make between  $A$  and  $B$  contacts during that visit, depending on the location. To be precise, we compute  $p$  as

$$p = \min\left\{1, \left[ \frac{A(B - A)(1 - e^{-N/\alpha})}{N - 1} \right] \right\} \quad (1)$$

for  $N \geq 2$ .

We use the values  $A = 5$ ,  $B = 40$  and  $\alpha = 1000$  for the runs described in this simulation, as chosen by calibrating against POLYMOD data [33].

4) *Transmission Model*: Disease transmission can result from contacts between susceptible and infectious individuals at a location. The transmission model is responsible for determining whether or not a given potential transmission occurs. Transmission probabilities depend on the susceptibility of the susceptible person's disease state,  $\sigma(X_i)$ , that of the individual infectious person,  $\beta_\sigma(p_i)$ , the infectivity of the infectious person's disease state,  $\iota(X_j)$ , that of the individual person,  $\beta_\iota(p_j)$ , the duration of the contact,  $T$ , and a global tuning value,  $\tau$ .

Under the assumption of independence of transitions across contacts, we define the *propensity*  $\rho$  of a contact between two people  $i$  and  $j$  as follows

$$\rho(i, j, T) = T \cdot \tau \cdot \beta_\sigma(p_i) \cdot \sigma(X_i) \cdot \beta_\iota(p_j) \cdot \iota(X_j) \quad (2)$$

where  $\tau$  is a tuning parameter proportional to the likelihood of becoming infected by being in contact with a single susceptible individual for one a second.

In order to determine whether or not a transition occurs for a given susceptible person  $p_i$  at the end of a time step, we sum the propensities from all  $m$  contacts  $p_i$  had with infectious people during the time step

$$A(p_i) = \sum_{j=0}^{m-1} \rho(X_i, X_j, T_j) \quad (3)$$

where  $T_j$  is the duration of the  $p_i$ 's  $j$ -th contact. We then sample a random number  $a \sim -\log(\text{uniform}(0, 1))/A$  and if  $a$  is less than one, the person will be infected. The probability of an infection occurring for a given person,  $p_i$ , is thus given by  $1 - e^{-A(p_i)}$ .

5) *Intervention Model*: Interventions have three main components: a trigger, a selector, and an action. The trigger activates the intervention at the end of a time step in response to some global condition, such as the population passing a case threshold. Once the intervention is active, its selector determines which people or locations it will apply its action to, based on their individual attributes and health states. This action will then either (1) add or remove some edges incident

---

## Algorithm 2: Parallel control flow in Loimos

---

```

1 Partition  $P$  into people partitions  $\mathbb{P} = \{P_i\}$ ;
2 Partition  $L$  into location partitions  $\mathbb{L} = \{L_j\}$ ;
3 for  $d \in \{1, \dots, d_{max}\}$  do
4   for  $P_i \in \mathbb{P}$  pardo
5     for  $p \in P_i$  do
6       foreach visit  $v$  in the visit schedule of  $p$  do
7         Send visit message  $m$  to location partition
8            $L_j : \ell \in L_j$ ;
9       end
10    end
11  end
12  for  $L_j \in \mathbb{L}$  pardo
13    for  $\ell \in L_j$  do
14      foreach message  $m$  destined for  $\ell$  do
15        Create an arrival and departure event for each
16        visit;
17        Put the events into the event queue  $Q_\ell$  of  $\ell$ ;
18      end
19      Reorder  $Q_\ell$  by the time of event in ascending order;
20      ComputeInteractions on  $Q_\ell$ ;
21      foreach person  $p$  who visited  $\ell$  do
22        Send exposure message  $m$  to people partition
23         $P_i : p \in P_i$ ;
24      end
25    end
26  end
27  for  $P_i \in \mathbb{P}$  pardo
28    for  $p \in P_i$  do
29      foreach message  $m$  destined for  $p$  do
30        Put the interactions into the interactions list  $I_p$  of
31         $p$ ;
32      end
33      ProcessInteractions on  $I_p$  to determine if an
34      infection occurred;
35      Update disease state  $d_p$ , if necessary;
36    end
37  end
38 end
39 Evaluate intervention triggers;

```

---

to the person or location in question or (2) adjust the values of attribute(s) of the person or location, which may be either used in later interventions or transmission propensity calculations. Most actions also can be reversed when the intervention no longer applies to the person or location in question.

At each step, these visits and exposures generate fine-grained communication to a number of other processes. Visit schedules are periodic unless changed by interventions, while the number of exposure messages is highly dependent on the specific mixture of infectious and susceptible people present at a given time in the simulation, as is the computational load involved in running the DES for each location. Consequently, the computation and communication in each step are highly irregular.

### B. Parallel Algorithm

The parallel algorithm, shown in (Algorithm 2), operates on a bipartite graph, with people and locations as nodes, and weekly visit schedules as edges, along with an assignment of people and locations to partitions. On each simulated day, each process first iterates over the people assigned to it, and each of their visits, sending a visit message to the process holding each visited location. People currently selected by an

TABLE II: Digital twin datasets generated and used for strong scaling studies. Interactions and visit counts given per week.

Dataset Name	Interactions	Visits	People	Locations
Maryland (MD)	486M	25.97M	5.513M	2.896M
Virginia (VA)	657M	36.20M	7.685M	4.092M
WS-20M	1.517B	840.0M	20M	5M
WS-100M	5.463B	4.200B	100M	25M
WS-US	14.97B	11.78B	280.4M	71.71M

active intervention may have an altered visits schedule (lines 4-10). Once all the visit messages have been received, arrival and departure events for each visit are created and placed in a time-ordered queue (lines 13-16). Each process performs a DES for each of its locations, as described in Algorithm 1, determines whether each pair of people whose visits overlap come into contact, and then computes the propensity of any contacts. Once the calculations have been performed, exposure messages are sent to the people that have been exposed (lines 19-21). These interactions are then processed to determine whether or not a given exposed person was infected (line 29). If a susceptible person is infected or an infected person makes a timed transition, their disease state will be updated to reflect this at the end of the simulation day (line 30). Finally, we evaluate the triggers of any interventions deployed in the current scenario (line 31).

#### IV. IMPLEMENTATION IN LOIMOS

We have developed a parallel epidemic modeling framework, Loimos, that implements the parallel algorithm described in the previous section. Loimos was written on top of the Charm++ [27], [28] parallel runtime. In this section, we present salient details regarding the flexible and modular design of the parallel implementation.

##### A. Inputs to the Simulator

Three core components define a complete epidemic simulation:

- 1) a population, consisting of people, locations, and visits
- 2) a disease, represented as an FSA, see Section III-A1
- 3) an (optional) intervention, capable of modifying visit schedules and disease transmission likelihoods

We used two different types of populations for the simulations described in this paper: realistic *digital twin* populations built to mirror the populations of several U.S. states, and purely synthetic populations.

1) *Generating Realistic Populations:* We generate these realistic datasets from a range of datasets through a pipeline based on that described by Barrett et al. [6]. When generating a digital twin for a given state, we start by constructing a collection of people with demographic data (including age, gender, and North American Industry Classification System (NAICS) code [15]) and partitioning these people into households in each U.S. Census block groups. These partitions are then refined through iterative proportional fitting until they match the distribution found in recent American Community Survey

TABLE III: Purely synthetic populations, used in weak scaling simulations.

Relative Size	People per Core	Locations per Core
1x	144k	36k
2x	288k	72k
4x	576k	144k

(ACS) Public Use Microdata Sample (PUMS) releases [14]. Next, each person is assigned an activity sequence where each activity has a type (e.g. home, work, etc), a start time, and a duration. This assignment is done based on National Household Travel Survey (NHTS) data [34] using random forest and classification and regression tree (CART) methods conditioned on demographic variables, and is calibrated against aggregated time-use surveys. Both residence and activity locations are then constructed using fusion techniques integrating Microsoft Building, National Center for Education Statistics (NCES) [21], and commercial data. Finally, people are assigned to residence locations, and activities to activity locations. This assignment is constrained to match ACS commute flow data and considers factors such as an individual’s NAICS code (ex: to ensure teachers work at schools). We use these techniques to generate the Maryland (MD) and Virginia (VA) datasets shown in Table II. These datasets are used for the configuration experiments described in Sections V-A-V-D and the strong scaling experiments described in Sections VI-VII.

2) *Purely Synthetic Population Generation:* Loimos additionally supports generating purely synthetic datasets which are either computed in advance or generated on the fly.

The precomputed synthetic datasets use the same input format outlined previously to represent a social network constructed from Watts-Strogatz small-world [42] random graph. Specifically, the random graph generated is treated as a location-location graph, which can be transformed into a people-location graph as follows:

- 1) Assign each location  $\ell$  a random number of people  $|P_\ell| \sim \text{poisson}(P/L)$ . Compute the total number of people generated,  $\hat{P}$ . If  $\hat{P} > P$  ( $\hat{P} < P$ ), select locations uniformly at random and remove (add) one person until  $\hat{P} = P$ , ensuring all location retain at least one person. We say these people call  $\ell$  their home location.
- 2) For each person  $p \in P_\ell$  assigned to  $\ell$ , for each day in the week, set aside  $t_{p,s} \sim \text{uniform}(6, 10)$  hours, centered around midnight, aside for sleep and partition the remaining time between  $|V_p| \sim \text{uniform}(5, 7)$  visits with start times chosen uniformly at random from  $p$ ’s non-sleeping hours. The destination for each visit is chosen by uniformly sampling with replacement from  $\ell$ ’s neighbors in the original location-location graph.

We use these people-location graphs to generate the large 20 million (WS-20M), 100 million (WS-100M), and 289 million (WS-US) datasets shown in Table II. We use these datasets for strong scaling runs in Sections VI-VII. Additionally, we propose that this synthetic graph generation method could

provide an accessible benchmark for interaction-based graph simulations.

When generating networks on the fly, Loimos uses a structured grid of locations to maintain epidemic locality. At runtime, users specify the grid width, grid height, population density (the number of people per location), and the average number of visits per person per day,  $\lambda_{visits}$ , via command line arguments to Loimos. People are then assigned to a home location uniformly throughout the grid. On each day, each person makes  $N \sim Poisson(\lambda_{visits})$  visits, with the  $i$ -th visit being to a random location  $d_i \sim Poisson(\lambda_{hops})$  hops away in the grid from their home location. For this work we use  $\lambda_{visits} = 5.2$  and  $\lambda_{hops} = 8$ . This synthetic structure produces the flexible population graphs shown in Table III. We use these graphs to test Loimos’s weak scaling performance in Sections VI-VII.

### B. Task-based Decomposition

Loimos is implemented in Charm++ [27], [28], a parallel language focused on asynchronous, message-driven programs. When writing Charm++ programs, the programmer organizes code and data into a combined object called a *chare*. Chares are in turn organized into *chare arrays*, indexable collections of chares. When the code is run, the Charm++ runtime is responsible for assigning chares to processors and for scheduling the execution of code on the various chares assigned to a given processor. This code is usually run in response to a message received from another chare. In Loimos, we use two chare arrays: one for people and one for locations, with each chare containing a partition of the appropriate data.

The other important object is a node group, an object which is instantiated once for each node the program is run on; node groups allow us to avoid keeping redundant copies of shared information in memory on one node, while also minimizing inter-node communication.

### C. Implementation of Different Models

The various models described in Section III-A are implemented modularly to better enable replacing them with alternative models.

1) *Disease Model*: At the start of a simulation, we load the FSA representing the simulated disease from an input file which specifies its states and transitions. A single copy of this information is stored on each node via Charm++ node group, as this allows each person and location chare to efficiently read-only access to these data. Other read-only data describing the input scenario is stored in a similar fashion.

When initializing the simulation, people begin in one of (potentially) several entry health states, as determined by their individual attributes, such as age, specified in the input file. They remain in this state until they are infected by an infectious person or chosen to seed the outbreak. At the start of the simulation, we select a small sample of people to infect during the first several days of the simulation. For the runs in this paper, we infect 10 people per day for the first week of the simulation.

2) *Discrete-event Simulation*: On each simulation day, the DES is triggered once the initial visit message exchange from people chares, which store the visit schedules for the people in the assigned partition, to location chares is complete. We use Charm++’s quiescence detection mechanism to determine when this exchange is done, as the number of visits a given location will receive is not known *a priori*, and is non-deterministic in the presence of any intervention which changes visits schedules, such as school closures. Once triggered, the DES for each location can be executed independently.

In implementing the DES algorithm, we made three key optimizations: (1) we only keep track of co-occupancy – and thus interactions – between susceptible between susceptible people and infectious people, (2) we only ever send interaction messages to susceptible people who had at least one interaction with an infectious person during a time step, and (3) exposure messages are sent as soon as we finish processing a susceptible individual’s departure event. Note that we are able to make this first change without affecting the results of the simulation because only contact between a susceptible person and an infectious person can cause an infection. The second optimization is especially helpful as in most iterations only a small fraction of visits will result in an exposure. These first optimizations have the side effect of making the computation and communication loads of the DES and exposure message exchange, respectively, highly dependent on the specific mixture of infectious and susceptible people visiting each location, which naturally varies over the course of the simulation. The third optimization allows us to significantly overlap computation and communication during this phase.

3) *Contact Model*: We implemented two different types of contact model in our code. The first is the *min/max/α* model discussed in Section III-A3. Since this requires knowledge of the maximum occupancy of each location, we implemented a pre-processing script to compute this based on the visit schedules file and save each location’s maximum occupancy to the locations file. At runtime, we read in this value for each location and compute the appropriate contact probability for each location while initializing each location at the start of a run and store it as a new location attribute. Since this cannot be computed in advance for the purely synthetic datasets, we implemented our second contact model, in which every location has the same contact probability.

4) *Transmission Model*: After each contact is identified, we compute the corresponding propensity immediately, and then batch it with the other exposure messages for the susceptible person involved. The exposure messages for each person are sent immediately when we process the departure event for their visit in the DES. Actual infections are not computed until after the DES is complete and all exposure messages received. We again use Charm++ quiescence detection to determine when this has occurred, as the number of exposure messages each person chare will receive is highly non-deterministic, depending on the mixture of infectious and susceptible people

TABLE IV: Architectural details of the platform used for the performance runs.

Name	Architecture	CPU	Cores/Node	Mem/Node	Network
Rivanna	Cray XC40	Intel Xeon Gold 6148	40	384 GB	EDR/FDR Infiniband

as well as the contact model. Once the message exchange is complete, each person chare sums the propensities for each person in their partition in order to determine whether or not they are infected.

5) *Intervention Model*: Similar to the disease model, the specifications for the interventions to be used in a given run are given in an input file and stored on a node group. Unlike the disease model, we store and update some state for each intervention which is updated by the main chare over the course of the simulation. In particular, at the end of each simulation day, we perform a reduction across all person chares to compute the number of total infectious people, and pass this value along with the current day to the triggers for each specified intervention to determine which interventions should be active. The ids for each active location-based intervention are then passed to all location chares. These chares then access the local copy of the intervention objects on their node and filter the locations assigned to that chare using the selector for the intervention, and apply the action to the relevant locations. Each intervention type is implemented as a separate class which extends a shared interface with containing methods for testing to see if a location should be selected, making arbitrary changes to a location’s state via an action, and undoing the changes wrought by the action. Some interventions, like vaccination, have a trivial undo method as the changes persist after the intervention ceases to be actively applied to them. A similar scheme is used for person-based interventions.

## V. ADDITIONAL PERFORMANCE CONSIDERATIONS

After implementing Loimos’s core features, we explored several avenues to further optimize our code’s performance. The two we found most beneficial were considering different combinations of processes and threads on each node, and static load balancing on the location data for realistic populations.

### A. Impact of Using Processes vs. Threads

The Charm++ suite includes support for different network layers, performance tools as well as abstractions that enable the programmer to adapt to the underlying hardware as a way to improve performance and scalability. All these components make Charm++ codes highly tunable. In particular, we are interested in analyzing how the symmetric multiprocessing (SMP) Charm++ mode behaves when compared to the non-SMP version for the Loimos code.

Enabling the Charm++ SMP mode is analogous to adding OpenMP or another shared memory parallel programming model to an MPI code, in that it runs multiple threads per process instead of the usual single thread. Note here that in either mode multiple chares can be – and usually are – assigned to the same thread. Users can specify how many worker threads

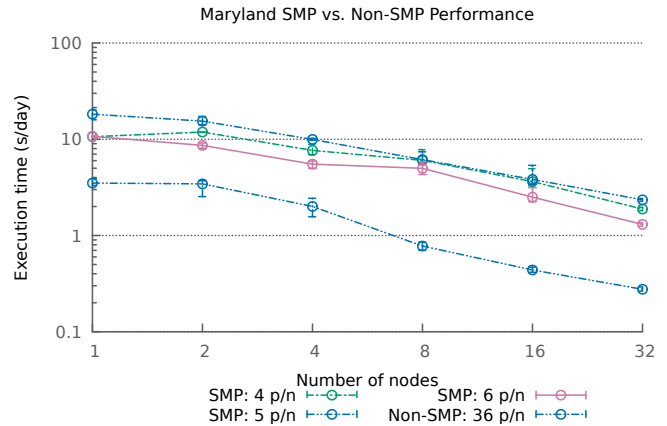


Fig. 1: Performance comparison of different SMP configurations, pairs of processes per node (p/n) and worker threads per process (t/p) vs a Non-SMP using one process per core (36 p/n) on the MD dataset. Execution times averaged over 5 runs, with extrema shown in error bars.

are spawned per process, along with an optional mapping from threads to cores, but one thread per process is always dedicated to communication. This communication thread manages inter-node messages whereas intra-node communication is managed through the shared memory address space common to all threads on the same node. The requirement of allocating one communication thread per process could be a disadvantage for computation intensive applications since compute cores have to be sacrificed. However, for communication intensive applications, the use of a dedicated communication thread to manage messaging might lead to better performance.

We set out to compare four different ratios of processes to nodes starting from 4 process to 6 processes per node in SMP mode and 36 processes per node in non-SMP mode, in each case leaving one core per thread. In order to do so, we performed a strong scaling experiment by running a 200 day experiment with five replicates in each cell. For this experiment, we used the MD dataset (see Table II) with static load balancing enabled. We conducted this experiment on Rivanna, where each physical compute node is comprised of 40 cores, but the scheduling policy only allows at most 37 cores on each node to be assigned to jobs.

Figure 1 shows the experimental results of this SMP vs Non-SMP comparison. Notice that the non-SMP configuration (solid line) consistently out-performs the SMP configurations (dashed lines). The non-SMP configuration also achieves a speedup of about  $\times 12.7$  when going from 1 node to 32, where the 4 p/n SMP configuration only has a .65, the 5 p/n configuration a  $\times 7.77$  speedup and the 8 p/n configuration



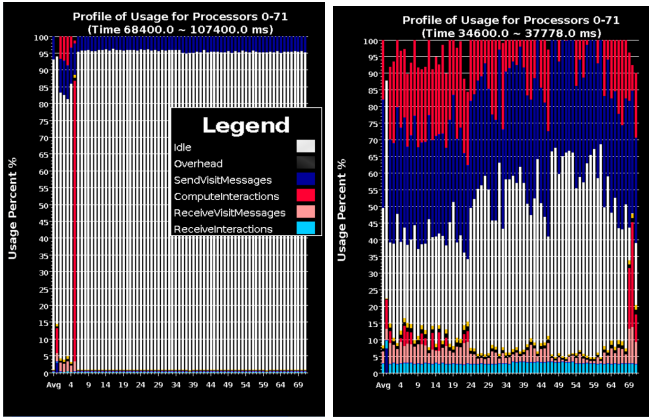


Fig. 2: Processor usage over one iteration of Loimos on 2 nodes with MD data and no optimizations (left), static load balancing only (right).

a  $\times 8.23$  speedup. As a result, we use the 36 p/n non-SMP configuration for all runs described in subsequent sections.

### B. Load Balancing

During initial runs of Loimos on the realistic datasets, we noticed that some processes ran much slower than others, as shown in the left of Figure 2. Since the bottleneck occurred in the ComputeInteractions function, which is computed on location chares, we set out to improve the assignment of locations to chares, in order to minimize the load on the heaviest chare.

Towards this end, we designed a simple static partitioning scheme meant to preserve location locality. First, we sorted all locations in the population by the id of their state, county, census tract, and census block group, in that order. This was intended to ensure that nearby locations were placed on the same chare if possible. Using the number of visits to a location as a proxy for load, we estimated the load for each partition,  $\lambda_p$ , as the ratio of visits to partitions, for a given number of partitions. Then, starting from the first location, we assign locations to partition 0 until the total estimated load exceeds  $\lambda_p$ , when we start assigning locations to partition 1, and so on until we reach the final partition, which receives the remaining unassigned locations. Note that this typically results in a few heavy locations assigned to their own chares. Applying this scheme drastically decreases the idle time on most processes, as shown in the right of Figure 2, although a much lower degree of imbalance remains. Figure 5 shows how Loimos’s performance improves (no-opt vs static) when using this static load balancing scheme. This produces a  $\times 5.47$  speedup for the MD data on 16 nodes.

### C. Message Aggregation

In subsequent runs, we noticed that we were experiencing significant overhead during both the visit and interaction message exchanges due to the large number of small messages we were sending. This can be seen on the left of Figure 3, where significant amounts of overhead (black) are visible where

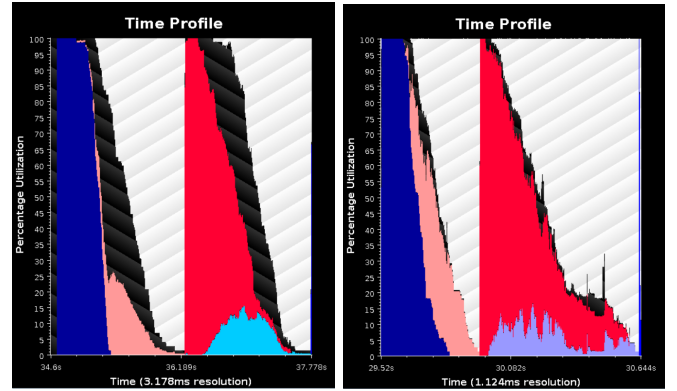


Fig. 3: Breakdown of time spent over one iteration of Loimos on 2 nodes with MD data and static load balancing only (left), and both static load balancing and message aggregation (right).

the SendVisitMessages (dark blue) and ReceiveVisitMessages (pink) methods overlap, as well as where the ComputeInteractions (red) and ReceiveInteractions (light blue) methods do. In order to mitigate this, we switched to using the Charm++ message aggregation utility for both message exchanges. The right of Figure 3 displays the reduced overheads we observed as a result, as well as the heightened level of overlap between the execution times of the two halves of the message exchanges. Figure 5 show the addition overall benefit of using message aggregation (static+agg) on top of the static load balancing scheme (static). This results in about a 28% speedup for the MD data on 16 nodes.

### D. Short Circuit Interaction Evaluation

Our final optimization was inspired by examining how the time we spent in each of the three main simulation phases varies over the course of a run. We had initially expected the time spent in the interaction computation phase to roughly track the number of infections, as more infectious people are present to interact with the existing susceptible population. Instead, we observed that the interaction phase dominated the runtime for the first half of the simulation, but fell to around the same level as the visit message exchange after the peak of the infection curve had passed, as shown by comparing the top and middle of Figure 4<sup>1</sup>. This corresponded to an increasing number of immune people in the population, who are ignored when identifying exposure interactions.

This lead us to realize that we were spending significant time computing interactions for every location even when no infectious individuals were present, as we still processed all susceptible arrival and departure events in the DES. In order to avoid this, we added a check to skip the interaction computation entirely on locations with no infectious people visiting them on a given day. As shown by comparing the top and bottom of Figure 4, after implementing this short circuit evaluation of the DES which computes interactions for each

<sup>1</sup>The periodicity of runtimes shown in the plot corresponds to the repetition of the base visit schedule each simulation week.



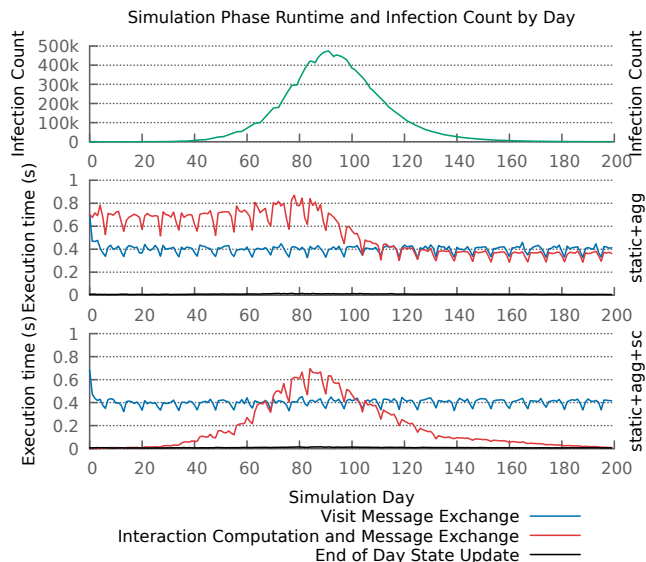


Fig. 4: One 200 day simulation of Loimos on 2 nodes with MD data and (top) infection counts and time spent in each simulation phase with (middle) only static load balancing and message aggregation, and (bottom) the addition of short circuit evaluation of interactions the over course of the run. Execution times averaged over 5 runs.

location the interaction runtime began to track the number of infectious people much more closely. Figure 5 shows how using this short circuit scheme (static+agg+sc) on top of the other two optimizations (smp+agg), for about a 19% speedup for the MD data on 16 nodes.

## VI. EXPERIMENTAL SETUP

We begin by performing extensive scalability studies using the 36 cores per node non-SMP configuration (See Section V-A) on Rivanna [2] at the University of Virginia. All scaling experiments were ran with Protobuf version 3.21.12 and Charm version 7.0.0. All scaling runs use the same random seed, and thus have identical epidemiological results. Values shown are the average of five replicates, with the error bars representing the minimum and maximum runtimes.

We use two large realistic datasets based on the populations of Maryland (MD) and Virginia (VA) and three larger purely synthetic dataset generated using the Watts-Strogatz algorithm (WS-20M, WS-100M, and WS-US) for a strong scaling experiment. The Maryland dataset is additionally used to validate Loimos’s simulation output against that of an established epidemiological simulation, EpiHiper [31]. See Section IV-A1 and Section IV-A2 for a more detailed description of these datasets. In combination with the contact model described in Section III-A3, these data allow us to model people-to-people disease spread through contacts.

Table II describes the number of people, locations, and total visits for all these datasets. Note that visits (person-location

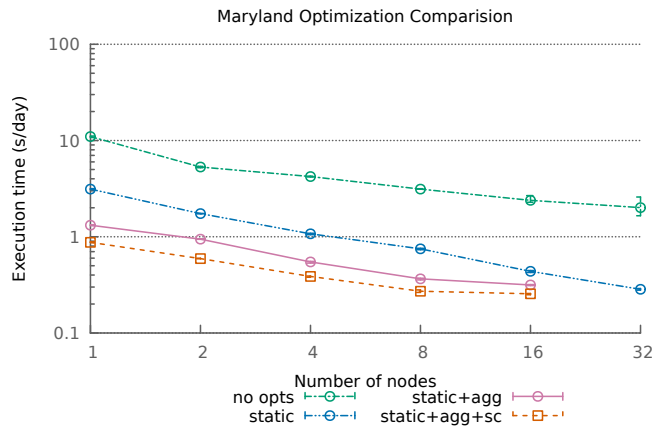


Fig. 5: Performance comparison of combinations of different performance optimizations: (1) static load balancing (static), (2) message aggregation (agg), and (3) short circuit evaluation of interactions (sc). Execution times averaged over 5 runs, with extrema shown in error bars.

edges) are repeated every seven days in the simulation and interaction (person-person edges) counts are given on average, due to the stochasticity of the contact model. We run the Maryland, Virginia, WS-20M, WS-100M, and WS-US datasets for 200 days total, processing a total of about 13.9, 18.7, 43.3, 156, and 428 billion interactions, respectively, over the course of the simulation. In order to ensure a representative workload, the transmissibility of the simulated outbreaks were tuned so that the number of infectious people peaked about halfway through the simulations.

Next, we performed a weak-scaling experiment. We ran three fixed problem sizes per working core, as shown in Table III. These datasets were generated using the on-the-fly synthetic population generation method outlined in Section IV-A2.

For all scaling runs, we evaluate the performance of runs by calculating the average execution time per simulation day. Note that this does not include data loading and application startup time.

Lastly, we perform a validation case study using the Maryland dataset also used for strong scaling. For 30 runs the random seed is allowed to vary in order to capture the full distribution of potential epidemiological outcomes. These results are then compared against runs of the existing EpiHiper simulation using the same input visit network and simple SIR disease model. Note that EpiHiper uses the visit data differently than Loimos: a preprocessing script determines the list and duration of contact for each person in the population, producing a fixed contact network which the disease then diffuses over. Each EpiHiper run is on a separate contact network. In contrast, Loimos determines a person’s contacts separately on each day, effectively resulting in a dynamic contact network, even in the absence of interventions. For all runs, the transmissibility is fixed at  $\tau = 0.05$  for both

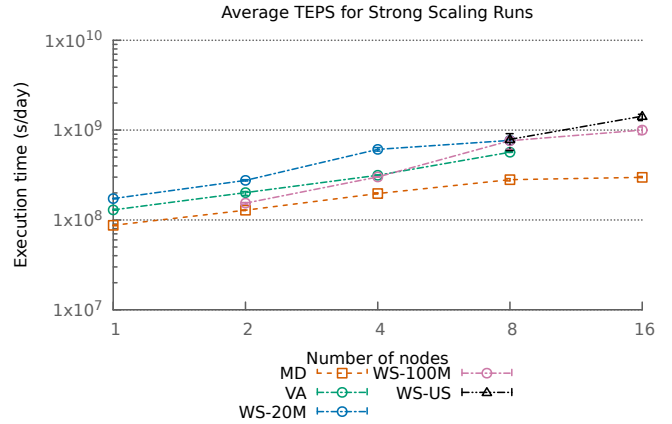
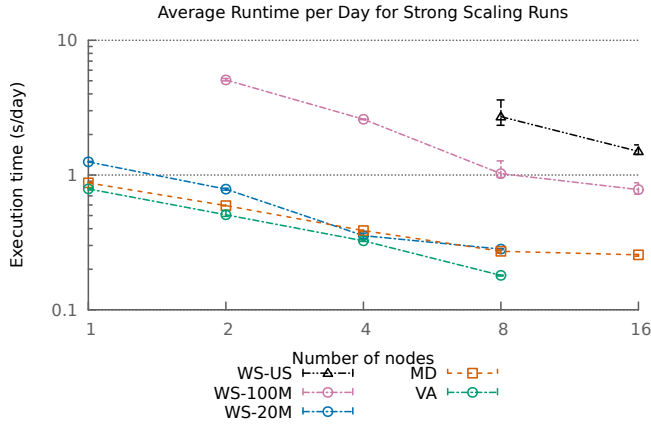


Fig. 6: Strong scaling performance of Loimos on Rivanna for five different datasets in terms of execution time (left) and traversed edges per second (TEPS, right). Execution times averaged over five runs, with extrema shown in error bars.

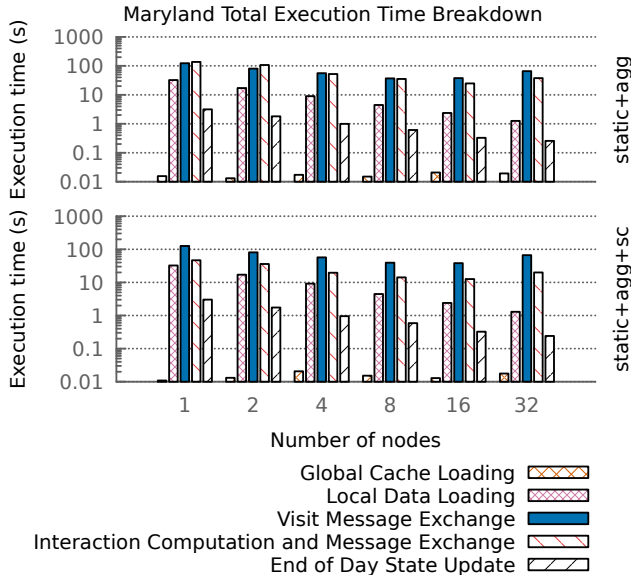


Fig. 7: Breakdown of total time spent in Loimos into different simulation phases (top) with only static load balancing and message aggregation, and (bottom) with short circuit evaluation of interactions.

simulations.

## VII. PERFORMANCE RESULTS

We now present scaling results from benchmarking Loimos using various inputs on Rivanna.

### A. Strong Scaling Performance

In order to understand how Loimos would enable large scale simulations we performed classical scaling analysis. Figure 6 shows the strong scaling results of the simulator when running the datasets listed in Table II.

For the average runtime (left), three of the five datasets – MD, WS-20M, and WS-US – scale to 16 nodes (576 cores),

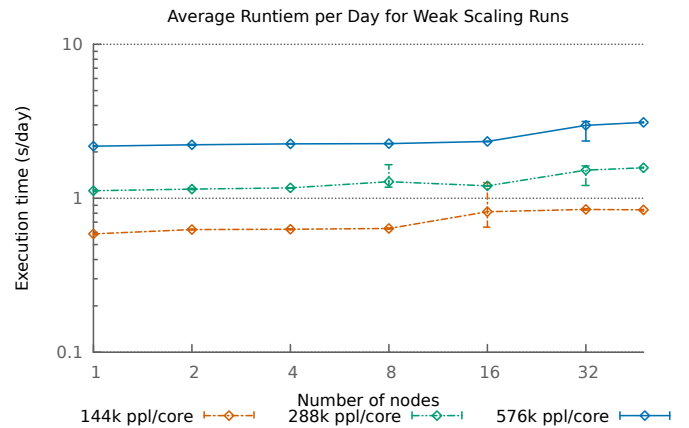


Fig. 8: Weak scaling results on Rivanna for three different per-processor loads. Execution times averaged over five runs, with extrema shown in error bars.

whereas the remaining two only scale to 8 nodes (288 cores). Notably, Loimos consistently runs faster on the VA data than the MD data, despite MD being a smaller state. When it comes to the traversed edges per second (TEPS, right), Loimos performs best on WS-20M through 4 nodes, after which point WS-US has the highest performance, peaking at about 1.4 trillion TEPS on 16 nodes (576 cores).

Figure 7 shows the breakdown of total time spent in Loimos into five main phases, which correspond to two data loading phases and the three parallel loops shown previously in Algorithm 2: (1) the initial visit message exchange (lines 4-10), (2) computing interactions and the resulting exposure message exchange (lines 11-23), and (3) the final health state updates (lines 24-32). We observe that without short circuit interaction computation, the runtime is roughly comparable between the visit and interaction phases (top), with the visits taking progressively more time as the node count increases, whereas with that optimization, the interaction phase consis-

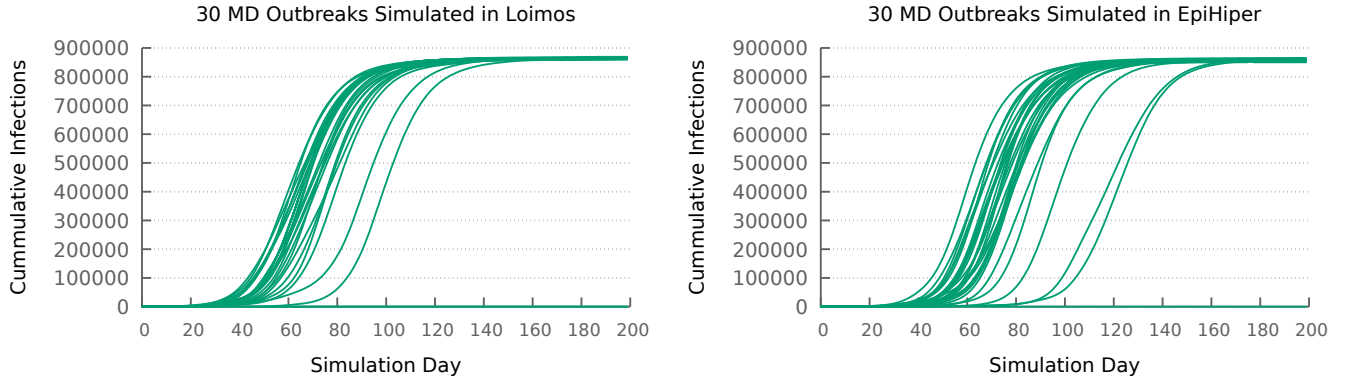


Fig. 9: Cumulative infections over time for 30 replicates in Loimos (left) and EpiHiper (right) of a simulated outbreak in Maryland.

tently takes less time than the visits phase. The runtime taken by local data loading decreases with node count in either case, with loading times approaching visit and interaction times on a single node but being reduced to a small fraction of the total runtime by 32 nodes. The time taken by the end of day update also decreases with node count, although it and the global cache phases take negligible time in all cases.

### B. Weak Scaling Performance

We also performed weak scaling tests to see how well Loimos handles datasets of increasing size. Figure 8 displays Loimos’s relatively flat weak scaling performance.

While these scaling results represent an optimistic representation of the person-location visit graph, they exploit location-load attributes that are present in real social graphs. While our simulation would see significant slowdowns from purely random visits, pre-run load balancing of real social graphs can similarly place people and locations together on processors such that there exists a high level of interconnectedness between these objects.

## VIII. INTERVENTION CASE STUDIES

Finally, we performed a validation case study to determine how Loimos’s epidemiological results compare with those of an established simulator, EpiHiper. Figure 9 shows how both simulators show similar overall disease trajectories, with outbreaks either persisting to infect a significant proportion of the population or dying out quickly, after infecting fewer than 100 people. In the former case, both simulations average similar numbers of total cumulative infections – 863k for Loimos and 858k for EpiHiper – and the latter occurs around the same number of times for each simulation – twice for Loimos and once for EpiHiper.

As for the timing of the persistent outbreaks, Loimos shows more tightly clustered results than EpiHiper. This is likely a byproduct of how the two simulators handle their input networks. Since EpiHiper uses the same contact network for an entire run, differences in the chosen contact network have the potential to cause compounding differences in the

simulation results. In contrast, since Loimos essentially selects a new contact network in each iteration, differences in contact networks between runs tend to be smoothed over to some extent as more networks are sampled over the course of a run, similar to how there is less variation in the average of 100 die rolls than that of a single roll.

## IX. CONCLUSION

Uncontrolled spread of infectious disease is a difficult problem to tackle, and one that requires policy makers to have the best possible tools in order to make informed decisions. Epidemic simulations are one such vital tool. The tight time constraints on relevant policy decisions mean that these simulations need to be able to model large regions extremely quickly and accurately across a wide variety of counterfactual scenarios. These demands require the use of powerful computing systems. We present a scalable parallel simulation framework for modeling contagion processes, Loimos, and demonstrate its capabilities.

In this work, we outlined the methods we used to develop this simulation framework and to optimize it for production HPC systems. We described the models underpinning our work as well as various optimizations we have made to enable the code to scale well. We demonstrate our code’s efficient use of resources during both strong and weak scaling runs on Rivanna, and show how the epidemiological results of the simulation compare to an existing simulator. Together, these runs demonstrate the potential uses of Loimos for policy makers as a fast, scalable epidemic simulator which is robust enough to capture the effects of policy interventions.

## ACKNOWLEDGMENT

This material is based in part upon work supported by the U.S. Department of Energy, Office of Science, Office of Advanced Scientific Computing Research, Department of Energy Computational Science Graduate Fellowship under Award No. DE-SC0021.

The authors acknowledge Research Computing at The University of Virginia for providing computational resources and

technical support that have contributed to the results reported within this publication. URL: <https://rc.virginia.edu>

## REFERENCES

- [1] "Covid-19 modeling." [Online]. Available: <https://www.vdh.virginia.gov/coronavirus/see-the-numbers/covid-19-modeling/>
- [2] "Rivanna." [Online]. Available: <https://www.rc.virginia.edu/userinfo/rivanna/overview/>
- [3] "Ut austin covid-19 modeling consortium." [Online]. Available: <https://covid-19.tacc.utexas.edu/>
- [4] B. G. Aaby, K. S. Perumalla, and S. K. Seal, "Efficient simulation of agent-based models on multi-gpu and multi-core clusters," in *Proceedings of the 3rd International ICST Conference on Simulation Tools and Techniques*, ser. SIMUTools '10. Brussels, BEL: ICST (Institute for Computer Sciences, Social-Informatics and Telecommunications Engineering), 2010. [Online]. Available: <https://doi.org/10.4108/ICST.SIMUTOOLS2010.8822>
- [5] C. Anastassopoulou, L. Russo, A. Tsakris, and C. Siettos, "Data-based analysis, modelling and forecasting of the covid-19 outbreak," *PLoS one*, vol. 15, no. 3, p. e0230405, 2020.
- [6] C. L. Barrett, R. J. Beckman, M. Khan, V. A. Kumar, M. V. Marathe, P. E. Stretz, T. Dutta, and B. Lewis, "Generation and analysis of large synthetic social contact networks," in *Proceedings of the 2009 Winter Simulation Conference (WSC)*. IEEE, 2009, pp. 1003–1014.
- [7] C. L. Barrett, K. R. Bisset, S. G. Eubank, X. Feng, and M. V. Marathe, "Episidemics: an efficient algorithm for simulating the spread of infectious disease over large realistic social networks," in *SC'08: Proceedings of the 2008 ACM/IEEE Conference on Supercomputing*. IEEE, 2008, pp. 1–12.
- [8] A. Bershteyn, J. Gerardin, D. Bridenbecker, C. W. Lorton, J. Bloedow, R. S. Baker, G. Chabot-Couture, Y. Chen, T. Fischle, K. Frey, J. S. Gauld, H. Hu, A. S. Izzo, D. J. Klein, D. Lukacevic, K. A. McCarthy, J. C. Miller, A. L. Ouedraogo, T. A. Perkins, J. Steinkraus, Q. A. ten Bosch, H.-F. Ting, S. Titova, B. G. Wagner, P. A. Welkhoff, E. A. Wenger, C. N. Wiswell, and for the Institute for Disease Modeling, "Implementation and applications of EMOD, an individual-based multi-disease modeling platform," *Pathogens and Disease*, vol. 76, no. 5, 07 2018, fty059. [Online]. Available: <https://doi.org/10.1093/femspd/fty059>
- [9] A. Bhatlele, J.-S. Yeom, N. Jain, C. J. Kuhlman, Y. Livnat, K. R. Bisset, L. V. Kale, and M. V. Marathe, "Massively parallel simulations of spread of infectious diseases over realistic social networks," in *2017 17th IEEE/ACM International Symposium on Cluster, Cloud and Grid Computing (CCGRID)*. IEEE, 2017, pp. 689–694.
- [10] P. Bhattacharya, J. Chen, S. Hoops, D. Machi, B. Lewis, S. Venkatramanan, M. L. Wilson, B. Klahn, A. Adiga, B. Hurt *et al.*, "Data-driven scalable pipeline using national agent-based models for real-time pandemic response and decision support," *The International Journal of High Performance Computing Applications*, p. 10943420221127034, 2022.
- [11] P. Bhattacharya, J. Chen, S. Hoops, D. Machi, B. Lewis, S. Venkatramanan, M. L. Wilson, B. Klahn, A. Adiga, B. Hurt, J. Outten, A. Adiga, A. Warren, Y. Y. Baek, P. Porebski, A. Marathe, D. Xie, S. Swarup, A. Vullikanti, H. Mortveit, S. Eubank, C. L. Barrett, and M. Marathe, "Data-driven scalable pipeline using national agent-based models for real-time pandemic response and decision support," *The International Journal of High Performance Computing Applications*, vol. 37, no. 1, pp. 4–27, Jan. 2023, publisher: SAGE Publications Ltd STM. [Online]. Available: <https://doi.org/10.1177/10943420221127034>
- [12] P. Bhattacharya, D. Machi, J. Chen, S. Hoops, B. Lewis, H. Mortveit, S. Venkatramanan, M. L. Wilson, A. Marathe, P. Porebski *et al.*, "Ai-driven agent-based models to study the role of vaccine acceptance in controlling covid-19 spread in the us," in *2021 IEEE International Conference on Big Data (Big Data)*. IEEE, 2021, pp. 1566–1574.
- [13] K. R. Bisset, J. Cadena, M. Khan, and C. J. Kuhlman, "Agent-Based Computational Epidemiological Modeling," *Journal of the Indian Institute of Science*, vol. 101, no. 3, pp. 303–327, Jul. 2021. [Online]. Available: <https://doi.org/10.1007/s41745-021-00260-2>
- [14] U. S. C. Bureau, "Census Bureau Data." [Online]. Available: <https://data.census.gov/>
- [15] U. S. C. Bureau, "North American Industry Classification System (NAICS) U.S. Census Bureau." [Online]. Available: <https://www.census.gov/naics/>
- [16] M. Chinazzi, J. T. Davis, M. Ajelli, C. Gioannini, M. Litvinova, S. Merler, A. P. y Piontti, K. Mu, L. Rossi, K. Sun *et al.*, "The effect of travel restrictions on the spread of the 2019 novel coronavirus (covid-19) outbreak," *Science*, vol. 368, no. 6489, pp. 395–400, 2020.
- [17] E. Y. Cramer, Y. Huang, Y. Wang, E. L. Ray, M. Cornell, J. Bracher, others, and U. C.-. F. H. Consortium, "The united states covid-19 forecast hub dataset," *medRxiv*, 2021. [Online]. Available: <https://www.medrxiv.org/content/10.1101/2021.11.04.21265886v1>
- [18] E. Cuevas, "An agent-based model to evaluate the covid-19 transmission risks in facilities," *Computers in biology and medicine*, vol. 121, p. 103827, 2020.
- [19] S. Eubank, H. Guclu, V. A. Kumar, M. V. Marathe, A. Srinivasan, Z. Toroczkai, and N. Wang, "Modelling disease outbreaks in realistic urban social networks," *Nature*, vol. 429, no. 6988, pp. 180–184, 2004.
- [20] N. M. Ferguson, M. J. Keeling, W. J. Edmunds, R. Gani, B. T. Grenfell, R. M. Anderson, and S. Leach, "Planning for smallpox outbreaks," *Nature*, vol. 425, no. 6959, pp. 681–685, 2003.
- [21] N. C. for Educational Statistics, "Electronic Catalog of NCES Products (National Center for Education Statistics). Publications and data products." publisher: National Center for Education Statistics. [Online]. Available: <https://nces.ed.gov/datatools/index.asp?DataToolSectionID=1>
- [22] T. C. Germann, K. Kadau, I. M. Longini, and C. A. Macken, "Mitigation strategies for pandemic influenza in the United States," *Proceedings of the National Academy of Sciences*, vol. 103, no. 15, pp. 5935–5940, Apr. 2006, publisher: Proceedings of the National Academy of Sciences. [Online]. Available: <https://www.pnas.org/doi/full/10.1073/pnas.0601266103>
- [23] G. Giordano, F. Blanchini, R. Bruno, P. Colaneri, A. Di Filippo, A. Di Matteo, and M. Colaneri, "Modelling the covid-19 epidemic and implementation of population-wide interventions in italy," *Nature medicine*, vol. 26, no. 6, pp. 855–860, 2020.
- [24] Google, *Protocol Buffers*, ver. 3.14.0, 2020. [Online]. Available: <https://github.com/protocolbuffers/protobuf/releases/tag/v3.14.0>
- [25] J. J. Grefenstette, S. T. Brown, R. Rosenfeld, J. DePasse, N. T. Stone, P. C. Cooley, W. D. Wheaton, A. Fyshe, D. D. Galloway, A. Sriram *et al.*, "Fred (a framework for reconstructing epidemic dynamics): an open-source software system for modeling infectious diseases and control strategies using census-based populations," *BMC public health*, vol. 13, no. 1, pp. 1–14, 2013.
- [26] H. W. Hethcote, "The mathematics of infectious diseases," *SIAM review*, vol. 42, no. 4, pp. 599–653, 2000.
- [27] L. V. Kale, A. Arya, A. Bhatlele, A. Gupta, N. Jain, P. Jetley, J. Lifflander, P. Miller, Y. Sun, R. Venkataraman, L. Wesolowski, and G. Zheng, "Charm++ for productivity and performance: A submission to the 2011 HPC Class II Challenge," Dept. of Computer Science, University of Illinois, Tech. Rep., Nov. 2011.
- [28] L. V. Kale and A. Bhatlele, Eds., *Parallel Science and Engineering Applications: The Charm++ Approach*. Taylor & Francis Group, CRC Press, Nov. 2013.
- [29] W.-m. Liu, H. W. Hethcote, and S. A. Levin, "Dynamical behavior of epidemiological models with nonlinear incidence rates," *Journal of mathematical biology*, vol. 25, pp. 359–380, 1987.
- [30] I. M. Longini, A. Nizam, S. Xu, K. Ungchusak, W. Hanshaoworakul, D. A. Cummings, and M. E. Halloran, "Containing pandemic influenza at the source," *Science*, vol. 309, no. 5737, pp. 1083–1087, 2005.
- [31] D. Machi, P. Bhattacharya, S. Hoops, J. Chen, H. Mortveit, S. Venkatramanan, B. Lewis, M. Wilson, A. Fadikar, T. Maiden, C. L. Barrett, and M. V. Marathe, "Scalable Epidemiological Workflows to Support COVID-19 Planning and Response," in *2021 IEEE International Parallel and Distributed Processing Symposium (IPDPS)*, May 2021, pp. 639–650, iSSN: 1530-2075.
- [32] MIDAS Network, "COVID-19 Scenario Modeling Hub," <https://covid19scenariomodellinghub.org>, last accessed Apr 6th, 2023.
- [33] J. Mossong, N. Hens, M. Jit, P. Beutels, K. Auranen, R. Mikolajczyk, M. Massari, S. Salmaso, G. S. Tomba, J. Wallinga *et al.*, "Social contacts and mixing patterns relevant to the spread of infectious diseases," *PLoS medicine*, vol. 5, no. 3, p. e74, 2008.
- [34] U. S. D. of Transportation Federal Highway Administration, "NHTS NextGen OD Data." [Online]. Available: <https://nhts.ornl.gov/od/>
- [35] J. Parker and J. M. Epstein, "A distributed platform for global-scale agent-based models of disease transmission," *ACM Transactions on Modeling and Computer Simulation (TOMACS)*, vol. 22, no. 1, pp. 1–25, 2011.

- [36] K. S. Perumalla and S. K. Seal, "Discrete event modeling and massively parallel execution of epidemic outbreak phenomena," *SIMULATION*, vol. 88, no. 7, pp. 768–783, 2012. [Online]. Available: <https://doi.org/10.1177/0037549711413001>
- [37] K. S. Perumalla and S. K. Seal, "Discrete event modeling and massively parallel execution of epidemic outbreak phenomena," *Simulation*, vol. 88, no. 7, pp. 768–783, 2012.
- [38] K. Prem, Y. Liu, T. W. Russell, A. J. Kucharski, R. M. Eggo, N. Davies, S. Flasche, S. Clifford, C. A. Pearson, J. D. Munday *et al.*, "The effect of control strategies to reduce social mixing on outcomes of the covid-19 epidemic in wuhan, china: a modelling study," *The Lancet Public Health*, vol. 5, no. 5, pp. e261–e270, 2020.
- [39] P. C. Silva, P. V. Batista, H. S. Lima, M. A. Alves, F. G. Guimarães, and R. C. Silva, "Covid-abs: An agent-based model of covid-19 epidemic to simulate health and economic effects of social distancing interventions," *Chaos, Solitons & Fractals*, vol. 139, p. 110088, 2020.
- [40] A. Tiwari, "Modelling and analysis of covid-19 epidemic in india," *Journal of Safety Science and Resilience*, vol. 1, no. 2, pp. 135–140, 2020.
- [41] S. Truelove, C. P. Smith, M. Qin, L. C. Mullany, R. K. Borchering, J. Lessler, K. Shea, E. Howerton, L. Contamin, J. Levander, J. Kerr, H. Hochheiser, M. Kinsey, K. Tallaksen, S. Wilson, L. Shin, K. Rainwater-Lovett, J. C. Lemairtre, J. Dent, J. Kaminsky, E. C. Lee, J. Perez-Saez, A. Hill, D. Karlen, M. Chinazzi, J. T. Davis, K. Mu, X. Xiong, A. Pastore y Piontti, A. Vespignani, A. Srivastava, P. Porebski, S. Venkatramanan, A. Adiga, B. Lewis, B. Klahn, J. Outten, M. Orr, G. Harrison, B. Hurt, J. Chen, A. Vullikanti, M. Marathe, S. Hoops, P. Bhattacharya, D. Machi, S. Chen, R. Paul, D. Janies, J.-C. Thill, M. Galanti, T. K. Yamana, S. Pei, J. L. Shaman, J. M. Healy, R. B. Slayton, M. Biggerstaff, M. A. Johansson, M. C. Runge, and C. Viboud, "Projected resurgence of COVID-19 in the United States in July–December 2021 resulting from the increased transmissibility of the Delta variant and faltering vaccination," *eLife*, vol. 11, p. e73584, Jun. 2022, publisher: eLife Sciences Publications, Ltd. [Online]. Available: <https://doi.org/10.7554/eLife.73584>
- [42] D. J. Watts and S. H. Strogatz, "Collective dynamics of 'small-world' networks," *nature*, vol. 393, no. 6684, pp. 440–442, 1998.
- [43] J.-S. Yeom, A. Bhatele, K. Bisset, E. Bohm, A. Gupta, L. V. Kale, M. Marathe, D. S. Nikolopoulos, M. Schulz, and L. Wesolowski, "Overcoming the scalability challenges of epidemic simulations on blue waters," in *2014 IEEE 28th International Parallel and Distributed Processing Symposium*. IEEE, 2014, pp. 755–764.